AMS Home   Journals Home   Journal Archive   Subscribe   For Authors   Help   Advanced Search   [Search] Go

Full Text View

Influences of Topography on the Modeling of Abyssal Water Masses. Part II: Spurious Extrema

Ross J. Murray and C. J. C. Reason

School of Earth Sciences, University of Melbourne, Parkville, Victoria, Australia

ABSTRACT

Unphysical extrema are found in ocean simulations employing space-centered advection even when horizontal mixing coefficients are sufficient to suppress checkerboard behavior. They are mostly found as isolated spurious temperature minima (density maxima) occurring in close association with topography and in places of concentrated upwelling or overflowing adjacent to the margins of deep basins, where velocities considerably exceed the vertical, or sometimes horizontal, grid Péclet condition. Temperature depressions may be as large as the expected temperature difference between levels and are capable of contaminating upstream water mass properties through horizontal diffusion and convective adjustment. Examples are discussed with reference to the finite difference solution for a stream of variable speed and diffusivity. Increased vertical resolution disproportionately reduces the magnitude but not necessarily the incidence of depressions. Flux correction eliminates the extrema and the contamination, but it can be very diffusive in the deeper layers and cannot overcome problems due to failure to resolve circulations.

1. Introduction

Space-centered advection has the advantage of being nondiffusive, but it is rather dispersive at high wavenumbers and requires explicit viscosity and diffusion to prevent the growth of variance at the grid scale. Weaver and Sarachik (1990) showed that a computational mode may be excited if the horizontal or vertical grid Péclet or grid Reynolds condition be exceeded. The grid Péclet conditions can be written

$$\mathrm{Pe}_H = u\Delta x/A_H \lesssim 2, \qquad \mathrm{Pe}_V = w\Delta z/K_H \lesssim 2,$$

where Pe_H, Pe_V, u, w, Δx, Δz, A_H, K_H are the horizontal and vertical grid Péclet numbers, velocities, grid spacings, and diffusivities, respectively. Such modes sometimes appear in horizontal fields, where they are recognized as checkerboarding, but the geostrophic coupling of momentum and tracer fields tends to inhibit this, and it is possible to set horizontal mixing parameters so that they do not arise under most conditions. Grid Péclet violations also occur in the vertical direction, but constraints on the thermohaline circulation allow less flexibility for adjusting diffusive coefficients in this direction. Violations can lead to the occurrence of unphysical extrema in the tracer fields and the production of spurious water masses. Weaver and Sarachik produced in a 12-level hemispheric model an anomalous overturning cell, which they ascribed to spurious dense water formation near the equator and which disappeared when the vertical resolution was increased to 19 levels.

In a companion study, which forms Part I of this work (Murray and Reason 1999), unphysical extrema were found to have a particular impact on bottom-water properties. This study investigated the effects on water properties of using different ways of representing fracture zone channels in the model topography below 3700 m. These channels are important in that they allow Antarctic Bottom Water (AABW) to pass through the submarine ridges from basin to basin in the Atlantic Ocean. The simulations were performed with a version of the Geophysical Fluid Dynamics Laboratory ocean model (described in Part I) that uses a longitudinally compressed horizontal grid of 300-km resolution (3° longitude × 2.5° latitude) in the Atlantic sector. Vertical diffusivity was set to $K_H = 1$ cm^2 s^{-1} (except in the uppermost levels) and horizontal diffusivity to $A_H = 1 \times 10^7$ cm^2 s^{-1}. Vertical grids of 12 and 21 levels were used, with thicknesses ranging from 25 m in the two uppermost layers to 900 m or 450 m, respectively, in the (3 or 6) layers lying beneath 1900-m depth. Below 160 m, each two layers of the 21-level grid occupied the depth range of one layer of the 12-level grid, and the topographic masks were constructed to keep the ocean volume of the two models the same.

In these models, the AABW was mostly confined to the depth range 3700–4600 m, which was represented by the bottom level of the 12-level grid and the bottom two levels of the 21-level grid. The topography was the same in all simulations above 3700 m, but differed below this level to allow fracture-zone channels to be represented in various ways. When channels were resolved in the model topography, water of Antarctic origin tended to spread through the basins via the channels at the bottom level(s). When they were not, the currents still flowed in a generally northward direction through the basins but were deflected upward along the margins and at the northern ends of the basins, where they were obstructed by the interbasin ridges. Spurious temperature depressions were found at some of these points of upwelling. These occurred with both open and closed channel topographies, and at both coarse and fine vertical resolutions; but the problem was particularly noticeable with blocked channel topography at coarse vertical resolution, and most of the discussion is concerned with results using this type of configuration. The simulations reported here all had blocked channels, but differed in the vertical resolution used and in the vertical or horizontal diffusivity applied at the bottom level. The model was formulated in the same way as in Part I, except that, to avoid our having to consider the impact of artificial source terms on the numerics, the bottom tracer restoration was suppressed. This did not affect the qualitative features of the extrema; however, without the restoration, the density contrast between the AABW and the North Atlantic Deep Water was greater, and in the NW Atlantic Basin there was a northward flow of Antarctic-influenced water, which upwelled at the northern end of the basin, causing a spurious depression there.

In the deep ocean, where vertical grid spacings are large but horizontal velocities are small, numerical violations are most likely to occur in the vertical direction; this contrasts with the situation in the upper ocean where the reverse is likely to be true. This is demonstrated by using the model parameters given above and some characteristic (standard deviation) velocities encountered in the 12-level simulations to calculate the ratios by which velocities exceeded the Péclet condition:

$$u = 5 \text{ cm s}^{-1} \qquad \text{(upper layers)} \qquad Pe_H/2 = 5$$

$$= <1 \text{ cm s}^{-1} \qquad \text{(lower layers)} \qquad = 1$$

$$w = 3 \times 10^{-4} \text{ cm s}^{-1} \quad \text{(upper layers)} \qquad Pe_V/2 = 0.3$$

$$= 3 \times 10^{-4} \text{ cm s}^{-1} \quad \text{(lower layers)} \qquad = 15.$$

The numbers given above imply that infringements of the grid Péclet condition in one or other direction occur just about everywhere in the ocean. That overshoots (which here also refer to undershoots) do not occur to a similar extent is due to the fact that the tracer solution is stabilized by diffusive fluxes in more than one direction and by dynamical feedbacks and to the fact that oscillations are only recognizable when the gradients in the grid wave are comparable to ambient tracer gradients. The grid Péclet condition is actually very severe, and an advective calculation that exactly satisfied it ($A_H = u\Delta x/2$) would, in fact, be equivalent to the very diffusive upwind or donor-cell scheme since

One matter that has not received much attention in the literature until now is the relationship between overshoots and topography. It is a fairly simple procedure to determine the points at which an unphysical tracer value occurs by comparing the tracer with its value at the same and the surrounding points at the previous time step(s). In the simulations that we have performed, nearly all spurious extrema were found to occur at isolated points lying next to topography. Most were associated with upward vertical velocities and cold (or, at any rate, *dense*) advection. Overshoots in downwelling regions are less likely since downwelling of sufficient intensity to lead to violations of the vertical grid Péclet condition is nearly always accompanied by convective adjustment, which effectively adds copious diffusion and negates any oscillatory tendency. However, in a vigorous density current, a violation in the horizontal can produce spuriously high densities in bottom cells or in convectively homogenized columns abutting topography.

Usually the amplitude of a computational mode is stabilized in one way or another (in the case of upwelling, by the temperature difference maintained between the water at the upper and lower levels); and, to some extent, one may be justified in saying that overshoots are "locked in" to particular locations relative to the topography. Provided that they do not grow, these overshoots will tend to remain local and static features of the solution; however, there are two things that may upset this and lead to contamination of the properties of the surrounding water. The first is that abnormally dense water may be mixed by convective adjustment into a lower level where it is no longer helping to maintain the oscillatory feature. The second, which is of more interest here, is that, to prevent the growth of wiggles, diffusion is required. For controlling the intensity of the thermohaline circulation, it is necessary to have a realistic vertical diffusivity; so, although the violation of the *vertical* grid Péclet condition is the cause of the overshooting, it is *horizontal* diffusion that is usually called upon to smooth out the oscillations caused by dispersion. However, it will be shown that this is ineffective in situations where the topography shields the horizontal flow from lateral warming and that, paradoxically, it is this horizontal diffusion that is *the cause of* the contamination.

The extent of this sort of contamination is illustrated in Fig. 1 ⊙▬, which shows the bottom level velocities and temperatures obtained using coarse resolution and normal diffusivities. As the AABW moves northward, it should warm as a result of diffusion of heat from the layer above, but it will be seen that temperatures monotonically *decrease* northward in each basin.

A number of methods may be used in an attempt to obviate this problem, but all of them have costs and drawbacks. There are some simple measures that reduce violations but may affect the solution in ways that work against the aim of modeling flows constrained by topography realistically. Duffy et al. (1997) found that increasing the horizontal viscosity eliminated spurious oscillations (manifested as "stacked jets" near the equator) by reducing horizontal divergences, and hence vertical velocities. We have found that increased viscosity reduces spurious extrema in the deep ocean too, but blurs and retards current features and makes the Antarctic overturning cell more dominant. Opening interbasin channels is another way of inhibiting spuriously low bottom temperatures, in this case by allowing warm diffusion through the gap, which counteracts cold advection in the upwelling water, and by allowing pressure gradient forces to adjust so that upwelling is less intense. This is appropriate where channels exist anyway and need to be included to improve the realism of the circulation generally, but is not justified where ridges, such as the Walvis Ridge, naturally block bottom water movement, and may not be possible along the margins or at the ends of trough systems where upwelling can also occur.

The remedy proposed by Weaver and Sarachik (1990) is to increase the vertical resolution. For many models, this may be a satisfactory measure. Increased resolution does, however, incur a proportionate increase in the computational cost. This is an important consideration in models that are to be used for long-term climate integrations, where the cost of improving the vertical resolution may have to be balanced against that of providing improved parameterizations, increased horizontal resolution, or longer integration times. An increase of vertical resolution from 12 to 19 or some other number of levels does not necessarily eliminate the incidence of spurious extrema; however, it certainly decreases their severity, and this in a nonlinear way that it is worth understanding.

Another approach is to include a monotonic or quasi-monotonic advection scheme. Two that have been used in ocean models are the upstream parabolic interpolation scheme of Leonard (1979) and the flux-corrected transport (FCT) scheme of Zalesak (1979). Both are essentially ways of modifying wall tracer values so as to provide a controlled mix of centred and upstream advection. Upstream advection, on its own, is nondispersive (and therefore monotonic) but very diffusive, so it is desirable that the upstream weighting should be limited. Leonard's scheme is not truly monotonic but contains sufficient effective diffusivity to damp oscillations in tracer fields rapidly. It has been adapted for use in the Bryan–Cox ocean model by Farrow and Stevens (1995), who showed it to be very effective in eliminating large horizontal temperature excursions in a fine resolution model of the Brazil–Falkland confluence. However, it may not perform so well near topography, where the upstream bias is lost.

FCT guarantees that overshoots shall not occur by applying just so much upstream advective tracer flux as is calculated necessary to prevent extrema from forming or becoming accentuated. Gerdes et al. (1991) incorporated the scheme in an ocean model and compared solutions for the North Atlantic Ocean using centered, upstream, and FCT advection. They

found that FCT used with isopycnal mixing produced a more realistic equatorial thermocline than did centered advection with horizontal mixing. Their Fig. 9 shows, however, that in the deep ocean, the effective vertical diffusivity is large and comparable to that of upstream advection. The effect of this may need to be considered in connection with abyssal water properties. Flux correction is computationally expensive, and it would be of interest to know how the costs and benefits of using it compare with those obtained from increased resolution.

The problem of numerical violations has become more acute following the adoption by many ocean modelers of the Gent–McWilliams parameterization (Gent and McWilliams 1990; Gent et al. 1995) and the attempt to use it with pure isopycnal diffusion. For the purpose of computing tracer advection in this parameterization, the explicit (or large scale) model velocities are augmented by eddy-induced transport velocities, which have the effect of flattening the density fields. This often magnifies total transport velocities, which may already be large in overflow regions. Groups using the scheme have been obliged to increase the number of vertical levels to about 20 to discourage spurious water mass formation (e.g., Danabasoglu et al. 1994; Hirst and McDougall 1996). Weaver and Eby (1997) have shown that the Gent–McWilliams scheme tends to produce spurious water masses in spite of increases in vertical resolution and have shown how flux correction can help. Although the transport velocities generated with eddy-induced transport may be larger and more noisy in some locations than without it, the spurious advection problem is essentially no different, and it is convenient to analyze it using a conventional model formulation. This also obviates a consideration of the effects of isopycnally oriented diffusion and the instabilities inherent in the Cox–Redi scheme (Griffies et al. 1998).

The purpose of this paper is to investigate how numerical problems are related to flows adjacent to deep topography and how they are affected by different model prescriptions. In section 2, the finite difference solution obtained for a simplified one-dimensional situation and predictions regarding the form of the solution and its sensitivity to vertical resolution and different advection methods are tested against some ocean GCM simulations. In section 3, the usefulness of alternative advection schemes for suppressing spurious extrema is considered.

2. Flow across a topographic barrier

a. Continuous solution

The upwelling of water over a topographic step is a situation in which a narrow, high-diffusivity, horizontal current is changed into a broad, low-diffusivity, vertical current and then back into a horizontal current again as the upwelling current merges with the flow at the upper level. This is one of a number of situations in which there is a variation of either speed or diffusivity along a flow trajectory. Other instances are large-scale upwelling (variation of K_H) and flow through a constriction (variation of speed). It is convenient to represent this type of flow as being insulated, nondivergent, unsheared, and time-invariant, having variable speed $u(x)$, cross section $h(x)$, and diffusivity $A(x)$ along a flow axis x, which may vary in direction. In the finite difference representation of the upwelling case, the trajectory axis, flow boundaries, and the grid interfaces might be as shown in Fig. 2 ⊙. In the figure, the current is shown as continuing toward the right of the plot after ascending the topographic barrier; however, the direction of the current after upwelling is not important. Some or all of it may, in fact, be deflected towards the left of the plot at the upper level, thus forming part of a large vertical convective cell. In practice, there will also be some diffusion and some water movement across the boundaries, as indicated by the dashed vectors in the diagram. However, the conceptual model is adequate for explaining the relevant aspects of the primitive equation model solution. Of particular interest is the relationship between the temperatures at the bottom of the step (T_b), at the top of the step (T_c), and far upstream (T_a).

The variation of temperature with x is first derived for the continuous case. Because the mass transport, $Q = hu$ is constant along the stream tube, the advective term, $-Q\partial T/\partial x$, may be written in flux form, and the advective–diffusive equation may be written

$$-\frac{\partial}{\partial x}(QT) + \frac{\partial}{\partial x}\left(hA\frac{\partial T}{\partial x}\right) = 0.$$

Integrating and dividing by hA, then substituting $u = Q/h$ and renaming the constant of integration gives

$$\frac{\partial T}{\partial x} = \frac{QT + \text{const}}{hA} = \frac{u}{A}(T - T_a), \qquad (1)$$

and hence

$$T(x) = T_a + T'(0) \exp \int_0^x (u/A) \, dx^*, \qquad (2)$$

where T_a is an upstream asymptotic value and $T'(0)$ [$=T(0) - T_a$] is the perturbation from T_a at $x = 0$. The integral and, hence, T are monotonic and continuous functions of x. Equation (2) may be substituted in (1) to give an explicit expression for the temperature gradient,

$$\frac{\partial T}{\partial x}(x) = \frac{u}{A} T'(0) \exp \int_0^x (u/A) \, dx^*,$$

which is equivalent in the constant velocity case to the less transparent expression derived by Cummins (1991) for the large-scale vertical density gradient.

In the case of constant cross section and diffusivity, the curve will be exponential. Where there is a sudden change of either u or A, there will also be a discontinuity of temperature gradient, which varies in proportion to u/A at the discontinuity. The inverse of this quantity, A/u, defines the scale length of the amplification.

In the application which is of interest to us, a horizontal bottom level current u of diffusivity A_H upwells in a vertical current w of diffusivity K_H. (Note that u and x now refer to the horizontal direction.) An example is taken from results from the 12-level blocked channel integration at the Rio Grande Rise near the location of the (blocked) Vema Channel (Fig. 1 ⊙). South of the ridge, the current is northward, with advective velocities characteristically of 0.1 cm s^{-1}; this is turned into an upwelling current of vertical velocity $w = u\Delta z/\Delta x \approx 3 \times 10^{-4}$ cm s^{-1}. Within each section, the cross section and the diffusivity are constant and the solution is exponential. The e-folding length scales for the two sections are

$$A_H/u = 1 \times 10^7/0.1 \text{ cm} = 1000 \text{ km} \quad (10° \text{ lat}),$$

$$K_H/w = 1/(3 \times 10^{-4}) \text{ cm} = 30 \text{ m}.$$

The effect of slackened velocity is more than offset by very low diffusivity in the vertical direction so that the short diffusive length scale and the strong tracer gradients are in the middle (upwelling) part of the trajectory. The continuous solution for this situation is depicted diagrammatically by the heavy curve in Fig. 3 ⊙. Because the vertical amplification scale is so much smaller than the upwelling depth (the 900 m between model levels), most of the temperature variation will occur close to the top, and the rest of the upwelling column and the whole bottom layer will be almost isothermal. While short advective–diffusive length scales are physically possible, they are not likely to be characteristic of flow over a topographic obstacle. In reality, an established flow across a topographic barrier would tend to align isothermal surfaces parallel to it, and strong gradients in the direction of the current would not occur. The problem in modeling this situation is that the overflowing stream might be quite shallow and there might be insufficient resolution to distinguish it from the ambient water above.

b. Finite difference solution

Let us compare this with how the temperature variation might be represented in a finite difference computation. The temperatures at three consecutive grid cells, $i - 1$, i, and $i + 1$, are T_{i-1}, T_i, and T_{i+1}. The spacing, stream width (or cross section), speed, and diffusivity between the first two are Δx_u, h_u, u_u, and A_u, and between the second two are Δx_d, h_d, u_d, and A_d. The subscripts $u = i - \frac{1}{2}$ and $d = i + \frac{1}{2}$ refer to the upstream and downstream interfaces, respectively. The advective–diffusive balance at the central cell, i, is

$$-\frac{A_u h_u}{\Delta x_u}(T_i - T_{i-1}) + \frac{u_u h_u}{2}(T_i + T_{i-1}) + \frac{A_d h_d}{\Delta x_d}(T_{i+1} - T_i)$$

$$-\frac{u_d h_d}{2}(T_{i+1} + T_i) = 0.$$

Dividing by $u_u h_u/2 = u_d h_d/2$ (by continuity) and defining $\text{Pe}_u = u_u \Delta x_u/A_u$ and $\text{Pe}_d = u_d \Delta x_d/A_d$,

$$-(2/Pe_u)(T_i - T_{i-1}) + (T_i + T_{i-1}) + (2/Pe_d)(T_{i+1} - T_i) - (T_{i+1} + T_i) = 0.$$

Subtracting $2T_i$ from the second term and adding it to the fourth, and grouping,

$$-(2/Pe_u + 1)(T_i - T_{i-1}) + (2/Pe_d - 1)(T_{i+1} - T_i) = 0;$$

whence

$$(T_{i+1} - T_i) = (T_i - T_{i-1})\left(\frac{2/Pe_u + 1}{2/Pe_d - 1}\right). \qquad (3)$$

For the case of constant Pe ($=Pe_u = Pe_d$), the temperature variation and stability condition have been derived more directly by [Weaver and Sarachik (1990)]. The temperature diverges in geometric progression from an asymptotic upstream value T_a, and it is convenient to denote perturbations from this value by primes, namely, $T'_i = T_i - T_a$; thus,

$$T'_i = \epsilon T'_{i-1}.$$

The amplification factor over one grid length is

$$\epsilon = e^{k\Delta x} = \frac{1 + Pe/2}{1 - Pe/2}, \qquad (4)$$

which gives a monotonic progression ($\epsilon > 0$) for Pe < 2 (the grid Péclet condition). The length scale of the amplification is

$$\frac{1}{k} = \Delta x / \log\left(\frac{1 + Pe/2}{1 - Pe/2}\right)$$
$$= \Delta x / [Pe + Pe^3/12 + O(Pe^5)], \qquad (5)$$

which rapidly converges to the continuous solution, $1/k = \Delta x/Pe = u/A$, as Pe$/2 \rightarrow 0$.

The amplifying behavior can be found for the case where there is a change of grid Péclet number. Subtracting T_a from all temperatures in [Eq. (3)] and using the expanded form of the interfacial subscripts,

$$T'_{i+1} - T'_i = (T'_i - T'_{i-1})\left(\frac{2/Pe_{i-1/2} + 1}{2/Pe_{i+1/2} - 1}\right). \qquad (6)$$

With an appropriate value of T_a, this is satisified by

$$T'_{i+1} - T'_i = T'_i \div (1/Pe_{i+1/2} - \tfrac{1}{2}),$$

that is,

$$T'_{i+1} = \epsilon_{i+1/2} T'_i. (7)$$

where

$$\epsilon_{i+1/2} = \frac{2/Pe_{i+1/2} + 1}{2/Pe_{i+1/2} - 1} = \frac{1 + Pe_{i+1/2}/2}{1 - Pe_{i+1/2}/2}. \qquad (8)$$

Since $Pe_{i+1/2} \geq 0$, $|\epsilon| \geq 1$; that is, the solution is continuously amplifying. Because T_a is the same for all i, the

amplification takes place about a constant asymptotic value; so

$$T_i' = \prod_{i^*=0}^{i-1} \epsilon_{i^*+1/2} T_0' = \exp\left(\sum_{i^*=0}^{i-1} k_{i^*+1/2}\Delta x_{i^*+1/2}\right)T_0',$$

which is the discrete analogue of the continuous equation [Eq. (2)]. Note the difference in the form of the amplification factor for the perturbation temperatures in Eq. (8) above, as compared to that appearing in the equation for the temperature differences [Eq. (6)], which also involves $Pe_{i-1/2}$. Since the *magnitude* of the perturbation is nondecreasing, the occurrence of an extremum at grid cell i depends only on the sign of $\epsilon_{i+1/2}$, and hence on the grid Péclet number at the interface immediately downstream. This means that if the grid Péclet condition be exceeded at only one point on a trajectory, there will be only one spurious extremum on it.

The above findings can now be related to the upwelling case described above. The diffusive length scale of the horizontal current is well resolved on the model grid, giving an exponential profile with an amplification length close to that of the continuous solution; that of the vertical current is not, the vertical grid Péclet number in this case being $Pe_V = w\Delta z/K_H \approx 30$.

Let T_b' $(=T_b - T_a)$ and T_c' $(=T_c - T_a)$ be the perturbation temperatures at the lower and upper points of the upwelling branch. Here T_b' is determined by T_c' (which can be taken as a boundary condition) by inversion Eq. (7),

$$T_b' = T_c'\left(\frac{1 - Pe_V/2}{1 + Pe_V/2}\right). \tag{9}$$

For $Pe_V > 2$, as it is here, T_b' will be negative (in this instance $T_b' = -0.88 T_c'$), so the exponential will curve downward, and the temperature of the corner cell will be a local minimum in the finite difference solution for the temperature variation versus distance along the flow axis; this is in contrast to the continuous solution, which does not admit of a change of the sign of the temperature gradient (see Fig. 3 ⊖). The minimum is just a single trough of the nonlocalized oscillation expected from Eq. (7) for $\epsilon < 0$. It is interesting that the temperature depression, T_b', is independent of the upstream (horizontal) grid spacing and diffusivity, and of whether these quantities be constant or variable.

To keep the model presented here simple, a vertical diffusive flux was only allowed between the two points in the vertical column that formed part of the trajectory. Without invalidating the condition for a computational mode, the formula will overestimate the depression of temperature at the corner point when there is vertical diffusion since this is normally applied at all grid points, irrespective of upward motion. When Pe is very large, temperature changes between grid points will be little affected by increases in u/A (in contrast to the situation when Pe is in the monotonic range and they are proportional to u/A). This being so, the contribution of vertical diffusion may been neglected, and
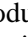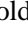
$$T_b' = -T_c'. \tag{10}$$

Consideration will show that Eq. (10) is necessary for advective equilibrium. The equation above makes the advective temperature in the upwelling face
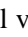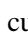
$$(T_a + T_c')/2 + (T_b + T_c')/2 = T_a,$$

which is the same temperature as that of the water entering at the other end of the abyssal basin; this ensures that the abyssal layer as a whole shall have no advective tendency, and therefore no tendency at all since there is no vertical diffusion into the bottom layer either.
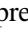
c. Ocean model experiments

Several experiments were carried with the 12-level model using normal diffusivities ($A_H = 1 \times 10^7$ cm^2 s^{-1}, $K_H = 1$ cm^2 s^{-1}) in most of the ocean, but with the vertical or horizontal diffusivity being varied at the bottom level. The vertical diffusivity between levels 11 and 12 was either normal or set to zero (except in convecting cells) and the horizontal diffusivity was either normal or increased to 2.5×10^7 cm^2 s^{-1} in level 12. The meridional variation of zonal average temperatures in the western Atlantic trough (comprising the Argentine, Brazil, and NW Atlantic Basins) is shown for each experiment in Fig. 4 ⊖.

The applicability of Eq. (10) is demonstrated by the curve for zero vertical diffusivity and normal horizontal diffusivity at level 12 (Fig. 4 ⬤▬, heavy solid curve). The features predicted from the one-dimensional model are all present in the curve for the Argentine Basin—the reversal of sign of the perturbation temperatures, the approximate equality of the magnitudes of T'_b and T'_c, and the length scale of the exponential (10° lat) in the horizontal. One would expect the profile normally to differ somewhat from the ideal exponential form owing to the fact that, even without any vertical diffusion, the upwelling is not confined to a single horizontal point. The upwelling at points upstream of the step (indicated by vertical dashed vectors in Fig. 2 ⬤▬) introduces cold advection, which tends to reduce or reverse the downward curvature of the temperature trace while still maintaining a monotonic negative gradient. In this case, the temperatures will be such that the calculated value of T_b will apply to the w-weighted average advective temperatures for the whole upwelling region. In the Brazil Basin (30°S–0°), much of the upwelling, and hence cold advection, is spread along the western margin of the basin, and this results in much of the temperature decrease happening in the southern half of the western boundary current, with the temperature gradient diminishing in the northern half. That the meridional trace still curves downward toward the Ceara rise is due to the movement of cold water around the northern end of the basin (as in the parallel simulation represented in Fig. 1 ⬤▬).

When normal vertical diffusivity was operating (Fig. 4 ⬤▬, heavy dashed curve), the temperature depression was less. This was expected, not only because of diffusion in the upwelling column [Eq. (9)], but also because the effective value of T_a would have been raised by the warming of the current due to downward diffusion at other points along and beside the current.

Spurious minima depress temperatures upstream by horizontal diffusion. The degree of contamination of the abyssal water may be taken to be proportional to the volume integral of the temperature depression in the bottom level, or, in the zonal-average profiles, the area of the curve beneath the T_a asymptote. In the ideal case of an exponential variation, this is $\int_{-\infty}^{0} T'(x)\, dx = -(A_H/u)T'_b$. If a larger horizontal diffusivity were used, the exponential would tail off more gradually, giving the temperature profile a smoother appearance and making the temperature depression less obvious. However, the equation implies that increasing the horizontal diffusivity (and also decreasing the current, which tends to happen at the same time) would actually *increase* the contamination by spreading the depression over a wider area. Some evidence of this is seen in the two light curves in Fig. 4 ⬤▬, which are for the simulations in which the horizontal diffusivity at the bottom level only was increased to 2.5×10^7 cm^2 s^{-1} (with and without vertical diffusivity between levels 11 and 12). The full effect of the spreading was not realized because the asymptotic value was not reached at the heads of the basins.

The extreme case of backward contamination occurs when the diffusivity becomes effectively infinite, as it does in convectively adjusting columns. The homogenization of tracer values represents a vanishingly small upstream decay of perturbation temperature over the length of the column. Convective adjustment normally takes place where negative buoyancy forcing at the surface creates static instability, but it may happen as a numerical artifact in stable upwelling columns. When rapid upwelling takes place over more than one grid length and the temperature at the top of the column is greater than that of the deep source water, that is, $T'_c > 0$, as is usually the case, the formulas predict a minimum temperature in the first cell below the top and an alternation of maxima and minima beneath it—this would be equivalent to the multiple wiggles sometimes found in horizontal fields. In practice, the pattern below the first minimum will be disrupted by convective adjustment, producing homogeneous columns. This was remarked upon with reference to the 21-level blocked ridge simulation in Part I, in which spurious minima were found in vertical pairs at levels 20 and 21. The phenomenon is more common in the 21-level than the 12-level simulations because of the way that the topography was stepped in pairs of levels and the greater incidence of upwelling columns of more than one grid length.

Temperature depressions in the 21-level simulation were found in the same places as in the 12-level simulation, but were much reduced in severity. A doubling of vertical resolution naturally leads to an approximate halving of grid Péclet numbers, but this is not a sufficient explanation for the size of the temperature response. The main examples of unphysical minima are associated with vertical velocities more than an order of magnitude greater than the grid Péclet limit, and it has been shown that the magnitude of the depression is almost insensitive to Pe_V under these conditions. However, with halved grid spacing, the natural temperature difference between levels, T'_c, will be about half, and hence so will T'_b at level 20. This is confirmed by the results of an experiment at 21-level resolution in which the vertical diffusivity was set to zero between levels 19 and 20 and between 20 and 21. Compared to the corresponding experiment at 12-level resolution, described earlier, the temperature depression was only about half (Fig. 5 ⬤▬). Because of convective mixing, the depression was not compounded in the next layer. A depression of even half the original size is still quite large; however, this only applied when vertical diffusion was suppressed. With normal vertical diffusion, the ratio was less again. In the basin interior, where upwelling is moderate, reductions in Pe_V have a greater effect on temperatures than at points of strong upwelling. The effective upstream temperature, T_a, is increased more than in the coarse resolution case, and this further lowers T'_c.

Convecting columns with spuriously low temperatures are found in overflow regions, where some upward currents occur amidst a general downward cascade. One example of a column homogenized in the bottom levels (two cells in the 12-level model and four in the 21-level model) was found in the Weddell Sea. The large vertical velocities at the top of the column and the fact that the depression of temperature relative to that at nearby grid points in the high resolution experiment was only half of that in the coarse resolution experiment showed clearly that the phenomenon was due to a violation of the vertical grid Péclet criterion. In overflow regions, currents may be sufficiently strong to exceed the horizontal grid Péclet criterion. Isolated minima have been found in corner grid cells southwest of Denmark Strait where the cell aspect ratio was such that velocities and grid separations caused violations at the southward outflow faces. In a separate experiment performed with stronger surface forcing in the Denmark Strait region, the temperature in the bottom four cells (depth 90– 800 m) of one vertical column in the 12-level simulation was a constant −3.9°C. With uniform column temperatures, it is not always immediately obvious what is causing the instability. A strong vertical current through the column (which interestingly was upward in these cases, not downward as one might expect) could create an oscillation, which would break up on account of static instability. However, the fact that the temperature was the same in the seven bottom cells at the same horizontal location in the 21-level simulation, shows that the cause of the problem was not coarse vertical resolution but strong horizontal cold advection, which was occurring over a number of levels.

3. Other advection schemes

a. Quadratic upstream interpolation

One scheme which has been used to overcome the problem of spurious oscillations is that proposed by Leonard (1979). Advective temperatures are given by the relation,

$$T_{i-1/2} = (3T_i + 6T_{i-1} - T_{i-2})/8,$$

where the current, u, is in the direction of increasing i. The parabolic interpolation gives more accurate wall values and less dispersion than linear interpolation for medium-long waves, and the upstream bias provides numerical diffusion that damps trailing oscillations. The equation for a forward time step, which he used, and including an explicit diffusion term is

$$T^{n+1}_i = T^n_i - (c/8)(3T_{i+1} + 3T_i - 7T_{i-1} + T_{i-2})^n + \Gamma(T_{i+1} - 2T_i + T_{i-1})^n,$$

where $c = u\Delta t/\Delta x$ and $\Gamma = A\Delta t/\Delta x^2$. An advective–diffusive balance may be obtained by equating T^{n+1}_i and T^n_i, setting $T_i = T_0 \epsilon^i$, and using Pe $= c/\Gamma$, namely,

$$(\epsilon - 1)(3\epsilon^2 + 6\epsilon - 1) - (8/Pe)\epsilon(\epsilon - 1)^2 = 0. \quad (11)$$

This equation has three roots: a background constant mode ($\epsilon = 1$) and a pair of modes given by

$$\epsilon = -\frac{6 + 8/Pe}{2(3 - 8/Pe)}\left[1 \pm \sqrt{1 + \frac{4(3 - 8/Pe)}{(6 + 8/Pe)^2}}\right].$$

One of these will be oscillatory if Pe $> 8/3$, which agrees with the curves shown in Fig. 23 of Leonard (1979). For the case of zero applied diffusion, the roots are ($\epsilon = -1 \pm 2/(3)^{1/2} = -2.154, 0.154$). With downstream boundary conditions, the solution is dominated by the growing, that is, oscillatory mode. In contrast to the computational mode generated by the centered difference solution, which is of constant amplitude, that generated by Leonard's scheme decays to 0.464 of its amplitude with each grid point in the upstream direction. This corresponds to a numerical diffusivity of $A_{num} = u\Delta x/Pe_{num}$, where

$$Pe_{num} = 2(\epsilon - 1)/(\epsilon + 1) = 5.464,$$

that is, to an upstream weighting of $2/5.464 = 0.366$. Because of the nonlinear nature of the calculation, the effective diffusivity (and hence the effective upstream weighting) becomes less as the explicit diffusivity is increased (e.g., for Pe = 0.5, $Pe_{num} = 20.4$).

Farrow and Stevens (1995) implemented Leonard's scheme into the Bryan–Cox ocean model with a predictor–corrector time step, namely,

$$T_i^{n+1/2} = T_i^n - (c/4)(T_{i+1}^n - T_{i-1}^n),$$

$$T_i^{n+1} = T_i^n - (c/8)(3T_{i+1} + 3T_i - 7T_{i-1} + T_{i-2})^{n+1/2}$$

$$(+ \text{ other terms}),$$

and some code that allowed for nonconstant grid spacings and ocean boundaries. The predictor step gives greater accuracy and stability in time, but introduces an extra factor, $[1 - (c/4)(\epsilon - 1/\epsilon)]$, into the advective term of Eq. (11). For $c \ll 1$, as it usually is, this exerts a small perturbation on the amplification of the dominant mode and gives rise to two additional modes ($\epsilon \approx 4/c, -c/4$), which decay rapidly upstream and downstream. A one-dimensional model run for 1000 time steps with a constant downstream boundary condition and zero applied diffusivity gave an oscillation with the same predicted amplification rate with both time integration methods. This shows that the extra amplifying mode was not used to suppress the oscillatory mode when the predictor–corrector time step was applied.

Unfortunately the damping properties of the advection scheme are not very useful in the case of a bottom current approaching and upwelling over a topographic step. Parabolic interpolation can only be applied where three upstream-biased grid points lie in a single physical coordinate direction. Where the $i - 2$ point does not exist, as is the case for an upwelling interface above a bottom cell, the scheme defaults to linear interpolation, that is, centered advection, giving an exit wall temperature that is too high. In the horizontal part of the trajectory, where the interpolation scheme *can* be applied, it will have little effect because horizontal diffusion is quite adequate for suppressing the computational mode there and keeping the tracer variation smooth. Thus, the conditions for a spurious temperature depression will still exist. (The same would hold for a horizontal grid Péclet violation following an overflow adjacent to topography.) The hypothesis has been tested with the one-dimensional model, this time with a constant downstream boundary condition, zero diffusivity in the interval adjacent to it, and Pe = 2 in the preceeding intervals. With forward time stepping, the depression was $-T'_c$, as with centered advection, and there was an exponential tail of almost the same steepness. With a predictor–corrector time step, the results were very similar, except that the depression was slightly attenuated (to $-0.922T'_c$).

b. Flux-corrected transport

Spurious extrema can be avoided by using an upstream advection scheme, which supplies sufficient diffusion to ensure monotonicity under all conditions but more than is normally necessary when fluxes in three dimensions are considered. In the algorithm of Zalesak (1979), each interfacial advective flux consists of an upstream and a centered part, the weighting being such as to satisfy some criterion of monotonicity. The procedure is, first, to determine, from the previous values of the tracer, a range of values in which the new value may fall without creating a new extremum or intensifying an existing one and, second, to calculate factors which limit the weighting of the centered part to that which just guarantees that advection on its own shall not exceed this range.

There is more than one way of determining the tracer range and choosing the flux limiters. Gerdes et al. (1991) defined the range as including the upstream solution at the central point and the surrounding time-centered interfacial-average values. Because the predominant transports, and hence the fluxes most needing correction, may lie in a direction almost perpendicular to that of greatest tracer variation, they first applied a one-dimensional (1D) prelimiter based upon the allowable tracer range and fluxes in each coordinate direction. Since thethree pairs of fluxes limited to ensure monotonicity individually might not do so in concert, allowance was made that the limiters might be further circumscribed by a three-dimensional (3D) limiter based on the full tracer range and fluxes in all directions, if desired.

Experiments were carried out with and without horizontal diffusion using FCT with 3D delimiters, FCT with 1D and 3D delimiters together, and also pure upstream advection. All of these used the blocked channel topography, in which the overshooting problem is most acute. Although both FCT schemes were found to be effective in eliminating extrema, they removed most of the evidence of an intermediate level salinity minimum and produced bottom temperatures in all experiments that were rather too warm. It made little difference to the solution whether or not the 3D delimiter was also applied. The effect of the warming on the bottom level meridional temperature variation can be seen in Fig. 6 ⊙. The FCT temperature profile follows a course midway between those of the centered and the upstream solution in which the temperatures were even higher. The characteristics described above seemed to indicate that too much correction, and hence diffusion, were being applied by the FCT scheme.

In order to establish the extent to which flux correction was being applied, numerical diffusion was diagnosed as the difference between the flux-corrected and centered advective tendencies. This was equivalent to the procedure of Weaver and Eby (1997). Flux correction was found to be occurring at *most* grid points in the ocean and with rms tendencies comparable to those of 3D advection and of horizontal diffusion at most levels. The flux corrections were also analyzed separately as horizontal and vertical numerical diffusion. In the bottom layer, the largest tendencies were in the vertical, of

the order of 5×10^{-9} °C s^{-1}, and associated with uplift at the northern ends of the basins. Numerical diffusion in both directions was slightly less with normal horizontal diffusion than without, but there was little difference between the solutions. Gerdes et al. (1991) calculated the added vertical diffusivity at each level using upstream advection and FCT.

Their results show vertical numerical diffusion to be as much as or slightly less than the applied diffusivity (0.65 cm^2 s^{-1}) in the upper ocean, but several times greater in the deep ocean, where it was comparable with numerical diffusion with upstream advection. This accounts for the fact that their scheme produced a sharper thermocline while at the same time excessively warming the deep ocean. Effective vertical diffusivities that we have calculated show very similar behavior. On the other hand, that of numerical horizontal diffusion was the opposite, with large corrections being needed in the upper oceans and only minor ones in the deep oceans. This accords with the arguments made in the introduction. Both horizontal and vertical numerical diffusivities were overall about one quarter of those diagnosed with upstream advection.

One of the problems with 1D prelimiters is that the limiters may be made very small (i.e., giving large upstream weighting) in a direction in which the tracer range is small but the flow is weak, resulting in larger than necessary upstream fluxes in a direction in which the range is larger but not of itself limiting. Other schemes for defining a range were tried, for example, using the central value and the transport-weighted average at the upstream cells and at the downstream cells, or (since spurious extrema are ultimately sensitive to antidiffusive downstream fluxes) just the central value and the downstream average. These attempts were unsuccessful. The essential difficulty is that allowable ranges and hence limiting ratios can only be calculated in relation to a whole grid cell from the combined effects of fluxes entering and leaving it; yet each of the fluxes to be limited affects two cells and does not necessarily individually cause a measurable excess of tracer range in either.

A simpler approach is just to apply 3D limiters without any consideration of direction, as originally envisaged by Zalesak (1979). When this was done, the incidence of flux correction was markedly reduced, occurring mainly near topography in places of marginal upwelling (vertical warm numerical diffusion from the level above) and at overflow points (horizontal warm numerical diffusion from the point ahead). At these particular locations, the corrections were of a magnitude similar to those found with 1D prelimiters. Elsewhere the corrections were much smaller or zero and tracer values were not much changed from the standard advection case. In that it has a very small diffusive effect on water properties overall, while still ensuring that isolated extrema in 3D will always be checked, the 3D-only method is useful for studying numerical problems in the bottom level, but no claims are made for its appropriateness in dealing with spurious oscillations in the ocean interior.

The 12-level 3D FCT simulations may be compared with the 21-level centered advection simulations. Both used the same normal explicit horizontal diffusion and blocked topography. The meridional profiles for the western Atlantic ocean (Fig. 6 ◉) in both experiments were similar to the standard 12-level centered advection case. The relative diminution of spurious minima in the higher resolution case has already been discussed. Temperatures averaged over the lowest two levels of the 21-level simulation (coinciding with the bottom level of the 12-level model) are slightly less than in the 3D FCT case;this may be due partly to (the small amount of) cold contamination at the bottom level in the centred advection experiment and partly to numerical diffusivity in the 3D FCT experiment. It is interesting that, with the excessive cold contamination of the standard experiment removed, the basin temperatures are about uniform and that the temperature jump is about half of that in the standard experiment. In the FCT experiment, this means that the flux-corrected, that is, upstream, advective temperature is the same as the space-centered advective temperature of the standard experiment. This being the case, it is not surprising that the temperature at the top of the ridge is about the same in the two experiments. This is as one would hope: flux correction has only eliminated the upstream contamination, without affecting the downstream solution.

4. Conclusions

The standard derivation of the grid Péclet instability criterion assumes a linear array of points with constant diffusivity and gives the condition for the appearance of a nonlocalized oscillatory mode. Multiple wiggles and checkerboarding are familiar in horizontal velocity and tracer fields in regions of strong currents when mixing coefficients have been set too low. But even when suitable coefficients have been used, extrema in 3D can still be found; they are nearly always produced at isolated points and in close association with topography. They often occur at the point where a horizontal bottom current deflects upward over a topographic barrier. In such locations there may be relatively little opportunity for diffusive interaction with points lying on either side of the current, and it may be appropriate to consider the solution as a function of distance along the trajectory.

The added ingredient here is a change of speed and/or diffusivity at some point along it. The continuous solution is a perturbation of constant sign and monotonically increasing magnitude about a constant asymptotic upstream value with an amplification factor u/A. The solution has the familiar exponential variation when this factor is constant. In the finite difference case, the perturbation is still of monotonically increasing magnitude, but not necessarily of constant sign. The amplification factor, related to grid index, is a function of Pe, and it is negative, that is, oscillatory, for Pe > 2. Although it is common to treat the oscillations as a wave phenomenon, the amplification and the conditions for an extremum are particular to the conditions between two grid points.

In strong upwelling, the vertical grid Péclet criterion may be exceeded by more than an order of magnitude. This is close to the nondiffusive limit, in which the oscillation will be of constant amplitude. When such upwelling occurs over a single grid interval, the temperature depression at the base will be as great as the expected difference in layer temperatures. When it extends through a column of several points, there will nearly always be just one point near the top of the column that satisfies these conditions and becomes abnormally cold and dense, the lower part of the column being made uniform by convective adjustment. Thus, multiple oscillations are unlikely to be found in vertical columns. Although the extrema themselves are isolated, their effects may be felt over many points upstream. The large diffusivity in the approaching part of the flow provides the means by which the spurious tracer value may contaminate water masses surrounding this point (by horizontal diffusion) or beneath it (by the enhancement of vertical mixing applied to statically unstable columns).

In the cases studied, the blocking of currents at the bottom level at a ridge did not actually prevent a continuous bottom current from flowing but did force it to rise to the next level to cross the ridge, where it was exposed to much mixing with the deep water at that level. It was this mixing that maintained the large vertical gradient in the direction of the upwelling. It does not seem likely that bottom-water currents in nature could overflow in the way they do in the model. However, even if they did, the low diffusivities and large gradients, which are characteristic of the vertical in the ocean, would not actually occur along the path of an overflowing current. Instead, a current would tend to align isopycnals parallel to itself, which would encourage mixing of temperature and salinity along them and shut out mixing with waters at the same level in the basins on either side. This is a situation that would probably be well represented by an isopycnal coordinate model (e.g., Oberhuber 1993), which is not constrained to representing the overflowing stream by a layer of any particular thickness. A more familiar and easily implemented alternative is a level model employing the Cox–Redi isopycnal diffusion scheme, although this suffers from the need for background diffusion and for slope limiting in regions of steep isopycnal gradients, which would very likely degrade its effectiveness in overflow situations. Griffies et al. (1997) have recently proposed numerics that would eliminate instabilities and, hence, the need for horizontal diffusion in the Cox–Redi scheme. In principle, one would expect any isopycnal diffusion scheme to inhibit the mixing of water masses of differing density, but this is only true in relation to diffusive mixing. Much of the mixing encountered in the model is due to the merging of currents in the vertical plane, and is therefore advective. In models of coarse vertical resolution, the isopycnals at deep levels are normally maintained sufficiently parallel relative to the grid by such processes that isopycnals cannot align with the particular current streams in which one may be interested, so advective instabilities associated with merging will still occur. Experiments similar to those described in this paper have been carried out using the Cox–Redi scheme, and the solutions show the same symptoms.

Various ways of overcoming the problem of spurious extrema have been considered. The scheme of Farrow and Stevens (1995) is probably not applicable to suppressing spurious extrema near topography. However, two ways that are effective for this are the use of increased vertical resolution and FCT. Both increase computational time by a similar factor (although the added proportional cost of FCT would be less with isopycnal mixing schemes since the overhead of using them is not increased by the FCT).

The 21-level model was designed to reproduce the ocean volume of the 12-level model, but with double the vertical resolution. The two simulations had a very similar climatology, except below 3700 m where there was an expected weakening of temperature depressions caused by numerical problems in the 21-level simulation. The improvement was not primarily due to the approximate halving of Pe_V at the most troublesome spots since at the high values obtaining there, the temperature depression is almost insensitive to this quantity; rather, it appears to have been due to the decrease in temperature differences between levels in upwelling columns, the initiation of convective adjustment in upwelling columns of more than one grid length, and the warming of the abyssal basins due to the lowering of Pe_V at basin interior points. Decreased vertical grid spacing does not eliminate numerical violations at this or any other particular resolution, but it does result in a more than proportionate decrease in the depression of temperatures: it has no direct effect on violations of the horizontal Péclet condition, such as have been found in polar overflow regions.

FCT, unlike increased resolution, guarantees freedom from violations, but at the price of creating extra diffusion. This is exaggerated in the deep ocean, where there are large grid spacings, producing excessive warmth there. The aim of FCT is to apply only so much upstream advection, in other words diffusion, as is necessary to prevent isolated extrema from developing. Because of the difficulty in designing a closure for the calculation of flux limiters, this aim has not been realized. It is probably still worth pursuing, using more elaborate schemes. For the purpose of this study, a simplification of the algorithm of Gerdes et al. that applies only 3D FCT was found to be of some use for removing isolated extrema near bottom topography while causing little change to tracers elsewhere; however, it is not expected that it would be of great benefit for removing extrema in the ocean interior if they were found to be a problem there.

Although both remedies answer the problem of eliminating numerical violations, there is a more fundamental concern that should guide our choice. Instabilities arise when a model attempts to calculate tendencies from gradients whose length scales are naturally too small to be resolved on the grid. To resolve the scales, extra diffusion is added to smooth the fields. FCT is just a way of adding this diffusion. Many features can stand some smoothing without losing their essential properties; in other cases they may not. Flows having different properties and going in opposite directions at adjacent levels will together

conduct a net advective heat transport. If the currents cannot be resolved they will be merged and will not be able to effect this transport. An FCT scheme will add sufficient diffusion to mix the converging water masses without distorting the water properties upstream. A centered advection scheme will maintain tracer variance by feeding this into oscillatory features, which because of dispersion do not propagate but distort the upstream solution. In neither case is the value at the point of mixing much affected since the two schemes are just different ways of providing the same advective flux through the interface to it. FCT may serve some purpose in that it will prevent the contamination of the upstream water mass, but it will not, of itself, achieve the onward transmission of the signal. Increased vertical resolution will do this to the extent that it allows counterflows to be resolved, or at any rate *better resolved* (i.e., with less mixing) than they would be at coarser resolution. A sensible approach would therefore be to modify the resolution or implement FCT depending on the way that flows resolve and spurious minima develop in the model solution.

REFERENCES

Cummins, P. F., 1991: The deep water stratification of ocean general circulation models. *Atmos.–Ocean,* **29,** 563–575..

Danabasoglu, G., J. C. McWilliams, and P. R. Gent, 1994: The role of mesoscale tracer transports in the global ocean circulation. *Science,* **264,** 1123–1126..

Duffy, P. B., K. Caldeira, J. Selvaggi, and M. I. Hoffert, 1997: Effects of subgrid-scale mixing parameterizations on simulated distributions of natural ^{14}C, temperature, and salinity in a three-dimensional ocean general circulation model. *J. Phys. Oceanogr.,* **27,** 498–523.. Find this article online

Farrow, D. E., and D. P. Stevens, 1995: A new tracer advection scheme for Bryan and Cox type ocean general circulation models. *J. Phys. Oceanogr.,* **25,** 1731–1741.. Find this article online

Gent, P. R., and J. C. McWilliams, 1990: Isopycnal mixing in ocean circulation models. *J. Phys. Oceanogr.,* **20,** 150–155.. Find this article online

—— ,J. Willebrand, T. McDougall, and J. C. McWilliams, 1995: Parameterizing eddy-induced tracer transports in ocean circulation models. *J. Phys. Oceanogr.,* **25,** 463–474.. Find this article online

Gerdes, R., C. Köberle, and J. Willebrand, 1991: The influence of numerical advection schemes on the results of ocean general circulation models. *Climate Dyn.,* **5,** 211–226..

Griffies, S. M., A. Gnanadesikan, R. C. Pacanowski, V. D. Larichev, J. K. Dukowicz, and R. D. Smith, 1998: Isoneutral diffusion in a *z*-coordinate ocean model. *J. Phys. Oceanogr.,* **28,** 805–830.. Find this article online

Hirst, A. C., and T. J. McDougall, 1996: Deep-water properties and surface buoyancy flux as simulated by a *Z*-coordinate model including eddy-induced advection. *J. Phys. Oceanogr.,* **26,** 1320–1343.. Find this article online

Leonard, B. P., 1979: A stable and accurate convective modeling procedure based on quadratic upstream interpolation. *Comput. Meth. Appl. Mech. Eng.,* **19,** 59–98..

Murray, R. J., and C. J. C. Reason, 1999: Influences of topography on the modeling of abyssal water masses. Part I: Effects of channel representation. *J. Phys. Oceanogr.,* **29,** 2851–2871.. Find this article online

Oberhuber, J. M., 1993: Simulation of the Atlantic circulation with a coupled sea ice–mixed layer–isopycnal general circulation model. Part I: Model description. *J. Phys. Oceanogr.,* **23,** 808–829.. Find this article online

Weaver, A. J., and E. S. Sarachik, 1990: On the importance of vertical resolution in certain ocean general circulation models. *J. Phys. Oceanogr.,* **20,** 600–609.. Find this article online

—— ,and M. Eby, 1997: On the numerical implementation of advection schemes for use in conjunction with various mixing parameterizations in the GFDL ocean model. *J. Phys. Oceanogr.,* **27,** 369–377.. Find this article online

Zalesak, S. T., 1979: Fully multidimensional flux-corrected transport algorithms for fluids. *J. Comput. Phys.,* **31,** 335–362..

Figures
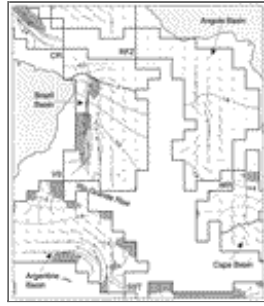
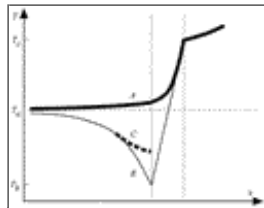Fig. 1. Bottom level temperatures (contour interval 0.2°C), horizontal velocities (1600 day streamlines), and upwelling regions. $(w > 4 \times 10^{-4}$ cm s^{-1} stippled) for a blocked channel simulation performed with normal diffusivities and no interior restoration. Blocked pathways include the Ceara rise (CR), Romanche Fracture Zone (RFZ), Vema Sill (VS), Walvis Ridge (WR), and South Sandwich Trench (SST).
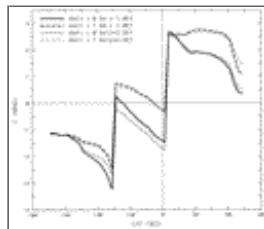
Fig. 2. A discretized representation of an upwelling flow trajectory, showing flow boundaries (heavy lines), flow axis (x), grid interfaces (cross section h), current speeds (u), and temperatures. The shaded box is a topography point and dashed vectors indicate possible cross-boundary currents that would exist in the nonideal situation.
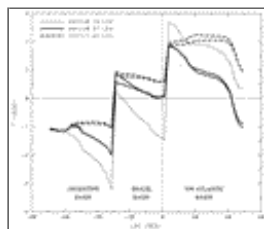
Fig. 3. Form of temperature variation along an upwelling flow trajectory. The three sections delineated by vertical dashed lines are (from left to right) the horizontal bottom flow, the upwelling into the next level, and the upper level continuation of the flow. Curve A is the continuous solution and curve B the discrete solution using centered advection. Curve C shows how the discrete solution may be modified when upwelling extends over a number of grid squares.

Fig. 4. Abyssal temperatures in the western trough for the 12-level blocked channel model, with zero and normal (1 cm^2 s^{-1}) K_H between levels 11 and 12 (solid and dashed lines) and with normal (1×10^7 cm^2 s^{-1}) and increased (2.5×10^7 cm^2 s^{-1}) A_H at level 12 (heavy and feint lines). Normal diffusivities applied at other levels.

Fig. 5. Temperatures in the western trough for the bottom level of the 12-level model with K_H being zero above that level (faint line), and for the bottom two levels of the 21-level model with K_H above those levels being zero (heavy solid lines) and normal (heavy dashed lines). Normal K_H applied at other levels and normal A_H applied throughout.
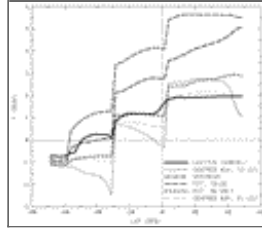
Click on thumbnail for full-sized image.

Fig. 6. Meridional profiles of abyssal (3700–4600 m) temperatures in the west Atlantic basins for Levitus, standard scheme (centered advection with 12 levels), upstream advection, 1D + 3D FCT, 3D FCT, and centered advection with 21 levels (depth average for two bottom levels). All simulations used normal horizontal diffusivity.

Corresponding author address: Mr. Ross J. Murray, School of Earth Sciences, University of Melbourne, Parkville, Victoria 3052, Australia.

E-mail: rjmury@met.unimelb.edu.au

top ▲